## International Journal of Thin Films Science and Technology

http://dx.doi.org/10.18576/ijtfst/140309

# Substituting sulfide by selenide in $CdSe_{1-x}S_x$ nano-films onto polymer substrate: Structural and optical properties

A. N. Abouelkhir <sup>1</sup>, M. Tag El-Dine <sup>1</sup> and E. R. Shaaban <sup>2,\*</sup>

Received: 16 Mar. 2025, Revised: 17 Jul. 2025, Accepted: 3 Aug. 2025

Published online: 1 Sep. 2025

**Abstract:** In this work, thin films of the ternary alloy  $CdSe_{1-x}S_x$  were deposited onto flexible polymer substrates using thermal evaporation, and their structural and optical characteristics were systematically analyzed. The study aimed to understand how progressive substitution of selenium with sulfur influences the crystalline structure, band gap, and optical parameters of the material. X-ray diffraction results confirmed that all compositions retained a hexagonal wurtzite phase, with increasing sulfur concentration leading to reduced crystallite size and enhanced micro strain attributed to lattice distortion caused by ionic size mismatch. Optical investigations using UV–Vis–NIR spectroscopy indicated a noticeable blue shift in the absorption edge, consistent with bandgap widening due to quantum confinement. The refractive index and extinction coefficient were extracted through Fresnel analysis and the Swanepoel method, both revealing a strong dependence on sulfur content. These findings highlight the potential of  $CdSe_{1-x}S_x$  films for integration into light weight and flexible optoelectronic systems, including solar cells and photodetectors, where material adaptability is essential.

**Keywords:**  $CdSe_{1-x}S_x$  thin film; flexible substrates; Structural analysis; Optical constants; classical and Swanepoel methods.

#### 1 Introduction

Binary semiconductors play a pivotal role in modern technology due to their broad applicability in various optoelectronic systems, including infrared (IR) sensors, photovoltaic devices, light-emitting diodes (LEDs), and laser technologies [1]. Among these, II-VI compound semiconductors, comprising elements from group IIB and group VIA of the periodic table, have attracted considerable research interest because of their favorable electronic and optical properties [2, 3]. Notably, compounds such as cadmium selenide (CdSe), cadmium sulfide (CdS), and their solid solutions offer potential for integration into high-performance devices [4,5].

The fabrication of thin films from II-VI compounds can be accomplished using several deposition techniques, including vacuum thermal evaporation, chemical vapor deposition (CVD), sputtering, and spray pyrolysis [6–8]. These methods provide control over film composition, thickness, and structural uniformity, all of which are essential for device optimization. The ternary alloy system  $CdSe_{1-x}S_x$  represents a class of semiconductors exhibiting both n-type conductivity typical of II-VI materials and, less frequently, p-type behavior under specific conditions. This solid solution features a direct band gap, tunable with composition, typically centered at around 2.7 eV at ambient temperature [9]. This makes  $CdSe_{1-x}S_x$  highly suitable for applications requiring bandgap engineering, such as full-color LEDs (red, green, and blue), solar energy conversion systems, laser displays, photochemical cells, and thin-film transistors.

The direct transition nature of  $CdSe_{1-x}S_x$  thin films is evidenced through spectroscopic studies [10], including absorption and photoluminescence spectra, which confirm that the extrema of the conduction and valence bands align at the center of the Brillouin zone (k=0). These materials offer the advantages of high absorption efficiency, chemical stability, and low production costs—factors that make them attractive for low-cost, polycrystalline solar cell applications, especially where marginally lower efficiency is acceptable in exchange for affordability [11].

<sup>&</sup>lt;sup>1</sup>Physics Department, Faculty of Science, New Valley University, Qena, Egypt

<sup>&</sup>lt;sup>2</sup> Department of Physics, Faculty of Science, Al-Azhar University, Assiut 71542, Egypt

<sup>\*</sup> Corresponding author e-mail: esam\_ramadan2005@yahoo.com



Conventional solar cells are commonly fabricated on rigid glass substrates, which, while offering mechanical stability, introduce several limitations. Glass is thermally insulating, leading to temperature gradients during annealing that can induce stress and fracture across large-area devices [12]. Moreover, the overall weight of glass-based modules reduces their viability in applications where weight is a constraint, such as aerospace and portable systems. In contrast, the deployment of thin-film solar cells on lightweight, flexible substrates, particularly metal foils or polymer films, offers substantial benefits. Flexible substrates [12, 13], often with thicknesses below 50 microns, contribute to a significant reduction in device weight and enhance the adaptability of the modules for non-planar or mobile installations. Furthermore, the use of such substrates simplifies system integration and reduces structural support requirements [14, 15].

This research focuses on the development and characterization of  $CdSe_{1-x}S_x$  thin films deposited on flexible polymer substrates. In particular, polymer acetate sheets were selected due to their thermal properties, featuring a thermal conductivity in the range of 0.16 to 0.36 W·m<sup>-1</sup>·K<sup>-1</sup> and a melting temperature near 564 K, which make them suitable for low-temperature film processing. The  $CdSe_{1-x}S_x$  films were synthesized using a controlled deposition method tailored to preserve substrate integrity while ensuring high film quality. The structural analysis was carried out using X-ray diffraction (XRD), enabling the determination of key parameters such as crystallite size, lattice strain, and phase composition as a function of sulfur content [16]. These findings provide insights into the effect of composition on microstructural evolution.

Optical properties were studied via UV-Vis spectroscopy, and refractive index dispersion was analyzed using Swanepoel's envelope method [10]. The correlation between structural parameters and optical constants such as refractive index, absorption coefficient, and optical band gap was established to understand the material's suitability for optoelectronic applications [17–19]. Furthermore, optical dispersion parameters were calculated to explore the interaction of light with the material in greater detail, offering a deeper understanding of the electronic structure.

# 2 Experimental techniques

To synthesize  $CdSe_{1-x}S_x$  nanostructures, high-purity reagents procured from Sigma-Aldrich Pvt. Ltd. were utilized, including cadmium chloride monohydrate (CdCl2·H2O), sodium sulfide (Na2S), and cetyltrimethylammonium bromide (CTAB). The synthesis of pure CdS nanostructures was carried out via a microwave-assisted technique. Initially, a 0.5 M aqueous solution of CdCl2·H2O was prepared by dissolving the salt in 50 mL of double-distilled water (DDW) in a clean glass beaker. Upon dissolution, the immediate formation of a pale-yellow precipitate was observed, indicating the initiation of cadmium-based compound formation. This solution was then transferred into cylindrical microwave-safe flasks and exposed to microwave irradiation at a power level of 700 W for 15 minutes. After completion of the heating cycle, the solution was allowed to cool naturally to room temperature. Following cooling, the product was washed multiple times with DDW to remove residual ions and by-products. The washed precipitate was then stirred at 70 °C for 10 minutes to ensure homogeneity; this intermediate was labeled as solution A. Subsequently, 0.5 g of CTAB was added to solution A and the mixture was stirred continuously for 30 minutes to facilitate the formation of a micellar environment, which plays a role in controlling the morphology of the resulting nanostructures. In parallel, a separate 0.5 M solution of Na<sub>2</sub>S was prepared in 50 mL of DDW, referred to as solution B. This solution was added dropwise to solution A under constant stirring to ensure controlled sulfide ion availability, promoting uniform growth of CdS nanoparticles. The final precipitate formed was collected, thoroughly rinsed with DDW, and dried. As a final step, the dried powders were annealed (calcined) at 100 °C. The purpose of this low-temperature annealing was to improve crystallinity and remove residual organic surfactants (such as CTAB), without inducing particle agglomeration or significant grain growth, which can occur at higher temperatures. Maintaining the annealing temperature at 100°C ensures the nanostructures retain their size and morphology while enhancing structural order.

Deposition and Characterization of  $CdSe_{1-x}S_x$  Thin Films:

Flexible polymer acetate substrates were used for the deposition of  $CdSe_{1-x}S_x$  thin films, which were fabricated via thermal evaporation in a high-vacuum environment (10-5 Torr) using molybdenum boats as evaporation sources. A consistent deposition rate was maintained throughout the process using an Edwards 306A thermal coating system. A quartz crystal monitor (FTM4), integrated with the vacuum chamber, was employed to accurately track the sulfur content and control the evaporation rate during film growth. The pressure during deposition was held steady at approximately 10-5 Torr.

To ensure film uniformity across the substrate surface, the sample holder was rotated at a speed of roughly 30 revolutions per minute (rpm) during deposition. The distance between the heated source and the substrate surface was



fixed at 21 cm to minimize direct thermal influence from the source. Elemental composition of the as-deposited films was evaluated using energy-dispersive X-ray spectroscopy (EDX), attached to a Philips XL scanning electron microscope (SEM). The SEM operated at an accelerating voltage of 30 kV, and the elemental analysis had a relative error margin not exceeding 2.2%. The crystalline structure of the films was investigated at ambient temperature using an X'Pert analytical X-ray diffractometer. The instrument operated with Cu K $\alpha$  radiation ( $\lambda = 1.540598 \text{Å}$ ), under tube conditions of 40 kV and 30 mA. XRD scans were recorded over a 20 range of 5° to 70°, using a step interval of 0.02° and a scan time of 0.4 seconds per step. Optical properties of the films, particularly transmittance T ( $\lambda$ ) and reflectance R ( $\lambda$ ), were measured across the spectral range of 400–2500 nm. These measurements were carried out at normal incidence using a JASCO V-670 double-beam UV–VIS–NIR spectrophotometer, enabling the evaluation of sulfur-dependent changes in optical behavior.

#### 3 Results and discussion

# 3.1 Structural Characterization of $CdSe_{1-x}S_x$ Nanoparticles

 $CdSe_{1-x}S_x$  nanoparticles were synthesized, and their structural characteristics were systematically examined as a function of sulfur content using X-ray diffraction (XRD), with the results presented in Fig. 1(a). The XRD patterns confirm that the synthesized powders possess a polycrystalline nature. The most prominent diffraction feature appeared at  $20 \approx 24.20^{\circ}$ , which corresponds to the (100) crystallographic plane. Additional reflections indexed to the (002), (102), and (103) planes were also observed and matched well with the standard reference data (see Fig. 1(b), JCPDS file). The dominant intensity of the (002) peak indicates a preferential crystal growth along this direction, and confirms that the material crystallizes predominantly in a hexagonal wurtzite phase. The structural phase remains unchanged with varying sulfur concentration; however, noticeable changes in peak intensity and width were observed. As the sulfur content increased, a progressive reduction in the intensity of the diffraction peaks was evident. This reduction can be attributed to the difference in atomic size between selenium (1.20 Å) and sulfur (1.04 Å). Substituting the larger Se atoms with smaller S atoms introduces localized strain and lattice distortions within the CdSe lattice. Such distortions can generate point defects or dislocations, which interfere with the regular atomic arrangement and increase X-ray scattering, thereby diminishing the intensity of the diffracted beams. Conversely, samples with lower sulfur content exhibited sharper and more intense peaks, suggesting fewer structural imperfections and improved crystallinity. Additionally, the XRD line broadening observed across all samples results not only from instrumental effects but also from intrinsic material factors, such as reduced crystallite size and micro strain. Variations in lattice constants with sulfur incorporation further support these structural modifications.

The microstructural parameters of  $CdSe_{1-x}S_x$  nanoparticles, such as the crystallite size (D) and microstrain  $(\varepsilon)$ , were evaluated using Scherrer's equation and the Williamson–Hall method, respectively, based on the full width at half maximum (FWHM), denoted as  $\beta$ , of the X-ray diffraction peaks [20, 21]:

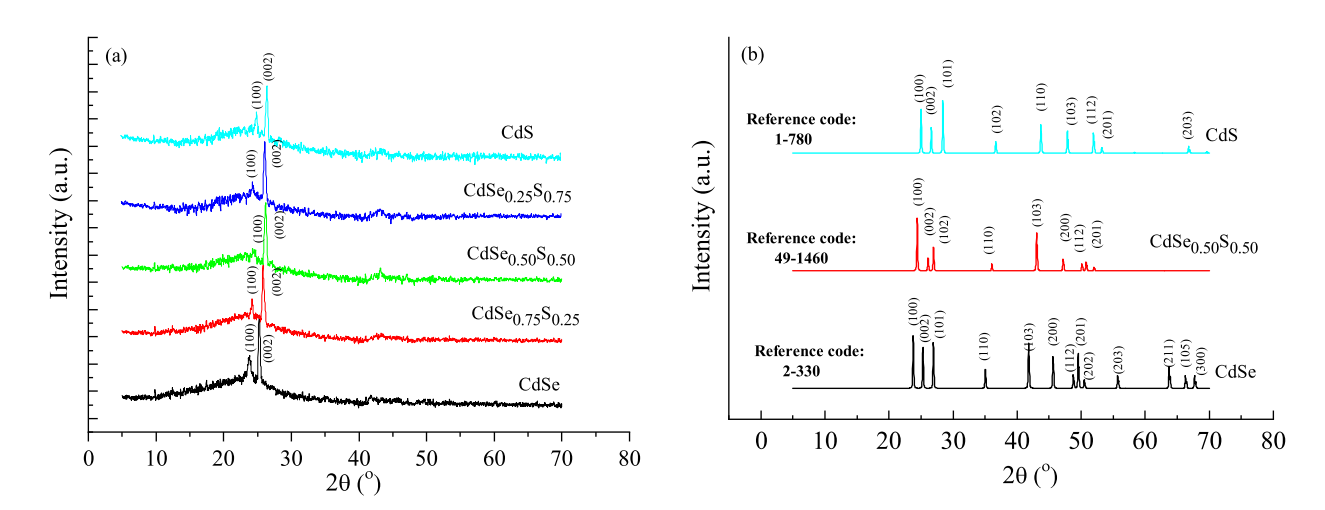
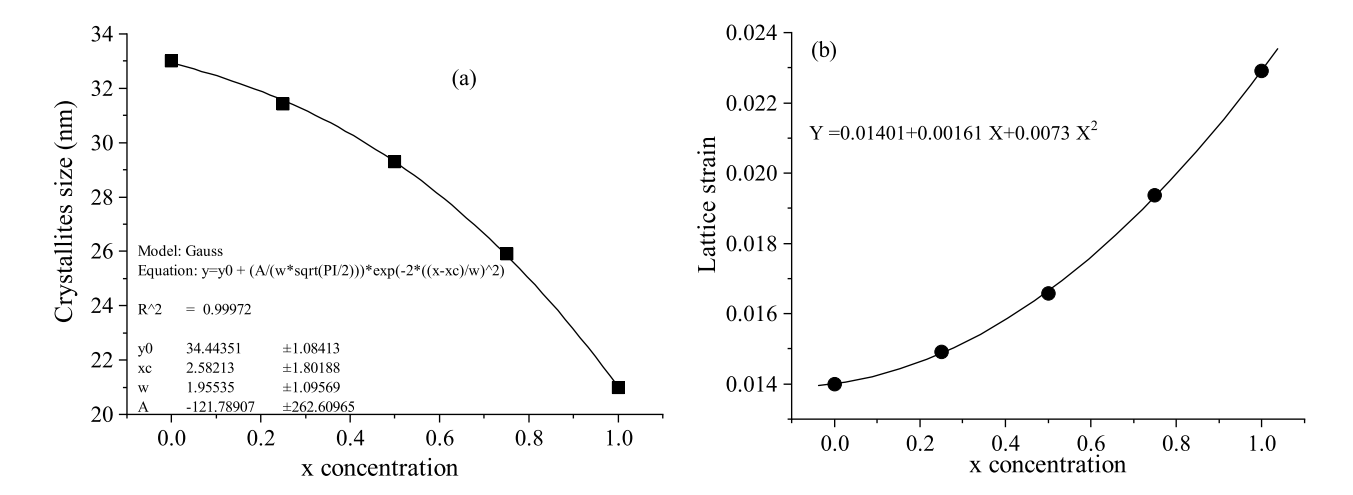


Fig. 1: (a) The XRD patterns of prepared  $CdSe_{1-x}S_x$  thin films onto flexible substrate and (b) JCPDS Data file for CdSe, CdSe0.5S0.5 and CdS.





**Fig. 2:** (a) The crystallite size and (b) Lattice strain of of  $CdSe_{1-x}S_x$  thin films.

$$D = \frac{0.9\lambda}{\beta\cos\theta} \tag{1}$$

$$e = \frac{\beta}{4\tan\theta} \tag{2}$$

$$\beta = \sqrt{\beta_{obs}^2 - \beta_{std}^2} \tag{3}$$

$$\frac{1}{d_{hkl}^2} = \frac{4}{3} \cdot \frac{h^2 + hk + k^2}{a^2} + \frac{l^2}{c^2} \tag{4}$$

where K is the shape factor (typically  $\approx 0.9$ ),  $\lambda$  is the X-ray wavelength,  $\theta$  is the Bragg diffraction angle, and  $d_{hkl}$  is the interplanar spacing corresponding to the (hkl) Miller indices.

The interplanar spacing was also calculated using Bragg's Law [22]:

$$2d_{hkl}\sin\theta = n\lambda\tag{5}$$

XRD analysis revealed that as the sulfur content (x) increases in  $CdSe_{1-x}S_x$  nanoparticles, the crystallite size (D) decreases, whereas the microstrain  $(\varepsilon)$  increases as shown in Fig. 2(a,b). This trend can be attributed to several interrelated physical effects: the first is sulfur atoms (atomic radius  $\approx 1.04$  A) are smaller than selenium atoms (atomic radius  $\approx 1.17$  Å). The substitution of larger Se atoms with smaller S atoms creates localized strain and lattice distortions, which restrict the long-range order of the crystal and hinder grain growth [23], the second, the difference in ionic radii and electronegativity between Se and S introduces defects and lattice imperfections. These structural distortions act as barriers to crystallite coalescence, thereby reducing crystallite size and enhancing internal strain [24]. The increasing microstrain causes a rise in internal energy within the lattice, which inhibits further grain growth during synthesis. This leads to a higher density of grain boundaries and smaller crystallites [25].

The hexagonal structure of  $CdSe_{1-x}S_x$  nanoparticles is defined by two main lattice parameters, a and c. These parameters were extracted using Eq. (4), by solveing for a and c if you measure the diffraction angle  $\theta$  for several known planes (hkl) using a known wavelength ( $\lambda = 1.5406$  Å). The variation of lattice parameters a and c with sulfur content (x) is presented in Fig. 3(a) and Fig. 3(b). Both parameters were found to decrease exponentially with increasing S concentration as follows. This decrease in lattice constants can be explained by the following: the Cd–S bond is shorter than the Cd–Se bond due to the smaller covalent radius of sulfur and stronger bonding. As S atoms replace Se in the lattice, the average bond length contracts, leading to a reduction in both a and c parameters [26, 27]. Also, as the smaller S atoms enter the crystal lattice, they effectively reduce the volume of the unit cell, contributing to the observed lattice parameter shrinkage [28]. Thus, increasing sulfur content in  $CdSe_{1-x}S_x$  nanocrystals leads to a systematic decrease in crystallite size and lattice constants, and a corresponding increase in microstrain an outcome that reflects the structural adjustment and energetic response of the lattice to compositional tuning.

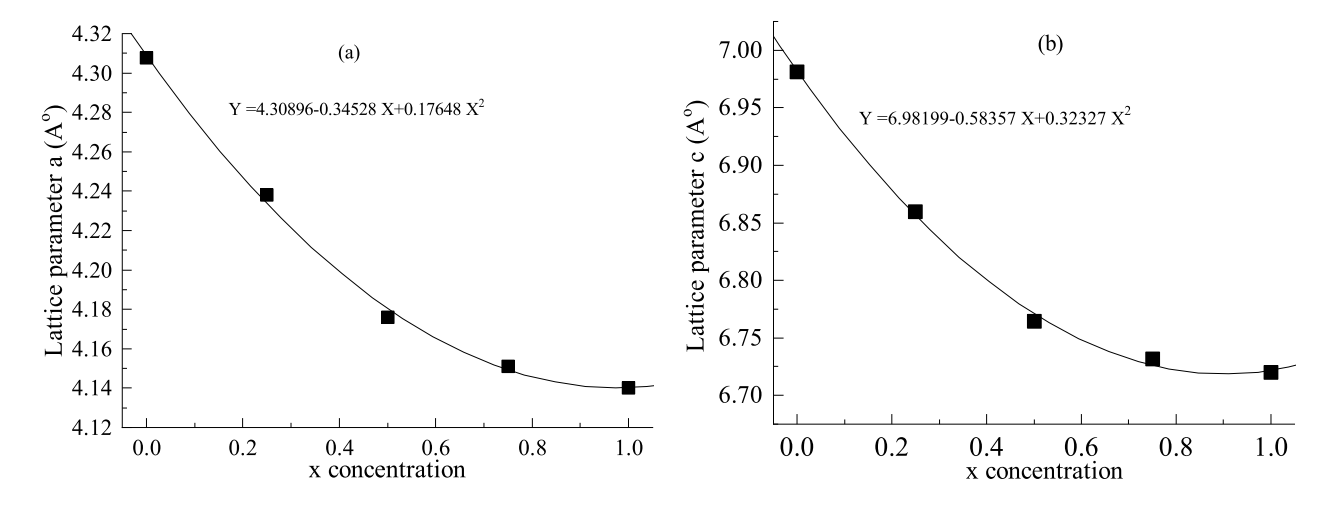


**Fig. 3:** The lattice parameter: (a) a and (b) c for  $CdSe_{1-x}S_x$  film in polymer substrates.

### 3.2 Optical Properties of $CdSe_{1-x}S_x$ Thin Films

Figure 4 presents the transmittance and reflectance spectra of  $CdSe_{1-x}S_x$  thin films over the wavelength range of 400–2500 nm. The transmittance spectra exhibit well-defined interference fringes, known as fringes of equal chromatic order (FECO), particularly at longer wavelengths. The presence of non-shrinking FECO patterns is indicative of the high optical homogeneity and surface smoothness of the deposited films, suggesting uniform film thickness and consistent refractive index across the measured area. Notably, for wavelengths exceeding 2000 nm, small oscillations begin to emerge in the spectra, and their amplitudes increase progressively with wavelength. This behavior is attributed to the thermal activation of interfacial inter diffusion between the  $CdSe_{1-x}S_x$  thin film and the flexible substrate, driven by the incident infrared (IR) radiation. The IR light provides sufficient energy to enhance atomic mobility at the interface, resulting in localized changes in optical properties and contributing to the observed oscillations. The size-dependent optical behavior of the films is further explained by quantum confinement effects. The variation in optical bandgap as a function of grain size can be described by a quantum confinement model, commonly expressed in the form:

$$E(R) = E_g + \frac{h^2 \pi^2}{2R^2} \left( \frac{1}{m_e} + \frac{1}{m_h} \right) - \frac{1.8e^2}{4\pi \varepsilon R}$$
 (6)

In this equation, ERy is the band gap energy of a nanocrystal with radius R, Eg is the bulk bandgap energy, me and mh are the effective masses of electrons and holes respectively,  $\varepsilon$  is the dielectric constant, and the final term accounts for the Coulomb attraction between charge carriers. The model includes three principal contributions: the quantum confinement (or kinetic energy) term inversely proportional to  $R^2$ , the Coulomb attraction term inversely proportional to R, and a confinement correction due to spatial localization. As particle size decreases, the kinetic energy term increases more significantly than the Coulomb term, resulting in a net increase in bandgap energy, a phenomenon manifested as a blue shift in the absorption edge. This shift becomes more pronounced with increasing sulfur content, which directly influences both the grain size and the electronic band structure of the  $CdSe_{1-x}S_x$  films. The optical transmittance spectra thus reveal a clear dependence on composition, highlighting the tunability of the bandgap through sulfur incorporation and nanostructural control.

#### 3.3 Energy Band Gap and Extinction Coefficient in the Strong Absorption Region

The optical absorption behavior of  $CdSe_{1-x}S_x$  thin films was analyzed in the strong absorption region to determine the optical band gap and extinction coefficient. The absorption coefficient ( $\alpha$ ) was calculated from the experimentally measured reflectance (R), transmittance (T), and film thickness (d) using the following relation [29]:

$$\alpha = \frac{1}{d} \ln \left[ \frac{(1-R)^2 + \left[ (1-R)^4 + 4R^2T^2 \right]^{1/2}}{2T} \right]$$
 (7)

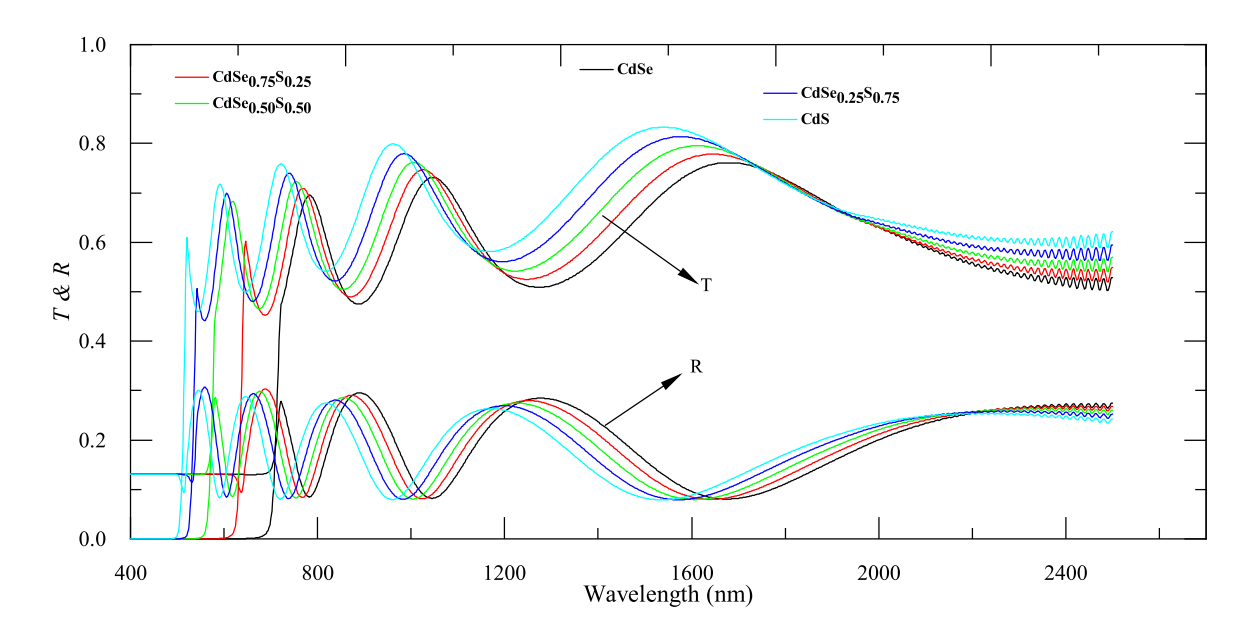


**Fig. 4:** The measured transmittance and reflectance spectra of  $CdSe_{1-x}S_x$  films/flexible substrates.

This expression is valid in regions where absorption is dominant and reflections from the rear surface are negligible or accounted for. The relationship between the absorption coefficient ( $\alpha$ ) and the incident photon energy (hv). Figure 5 provides insight into the type of optical transition, whether direct or indirect. The nature of the electronic transitions can be described by the Tauc relation [30]:

$$\alpha(hv) = \frac{K\left(hv - E_g^{opt}\right)^n}{hv} \tag{8}$$

In this expression: K is a material-dependent constant,  $E_g$  is the optical band gap energy, n is the exponent that characterizes the type of electronic transition:  $n=\frac{1}{2}$  for allowed direct transitions, n=2 for allowed indirect transitions. For the  $\mathrm{CdSe}_{1-x}\mathrm{S}_x$  thin films examined in this study, the plots of  $(\alpha h v)^2$  versus h v showed linear behavior in the strong absorption region, indicating that the electronic transitions are of the allowed direct type. Figure 7 presents representative Tauc plots for various compositions of  $\mathrm{CdSe}_{1-x}\mathrm{S}_x$  films ( $0 \le x \le 10$ ). The optical band gap for each sample was determined by extrapolating the linear portion of the plot to the energy axis at  $(\alpha h v)^2 = 0$  0 (see Fig. 6).

The extracted optical band gap values are shown in Fig. 8. A noticeable exponential growth increase in band gap energy is observed with increasing sulfur content (x) in the  $CdSe_{1-x}S_x$  alloy system. This trend is primarily attributed to two factors: the first, as the sulfur content increases, the crystallite size of the films tends to decrease. This size reduction enhances quantum confinement effects, which are prominent in nanoscale materials. In such confined systems, the energy levels become discretized due to the spatial restriction of charge carriers, leading to an increase in the effective band gap. When the particle size approaches or falls below the exciton Bohr radius, the energy required to excite an electron from the valence band to the conduction band increases. This effect causes a blue shift in the absorption edge and results in a higher observed band gap compared to bulk materials. The second is at the nanoscale, the number of atoms constituting each crystallite becomes significantly reduced, and the overlap of atomic orbitals that form continuous energy bands diminishes. This leads to a narrowing of both the valence and conduction bands, thereby increasing the separation between them. As a consequence, the energy gap widens further due to the reduced density of electronic states and diminished band dispersion. In addition, the incorporation of sulfur into the CdSe lattice leads to an increase in the electronegativity and lattice strain, both of which can influence the band structure and contribute to the observed variation in the optical band gap. These findings confirm that compositional tuning in the  $CdSe_{1-x}S_x$  system provides an effective method for engineering the optical properties of the films, particularly in applications where precise control of the band gap is required.



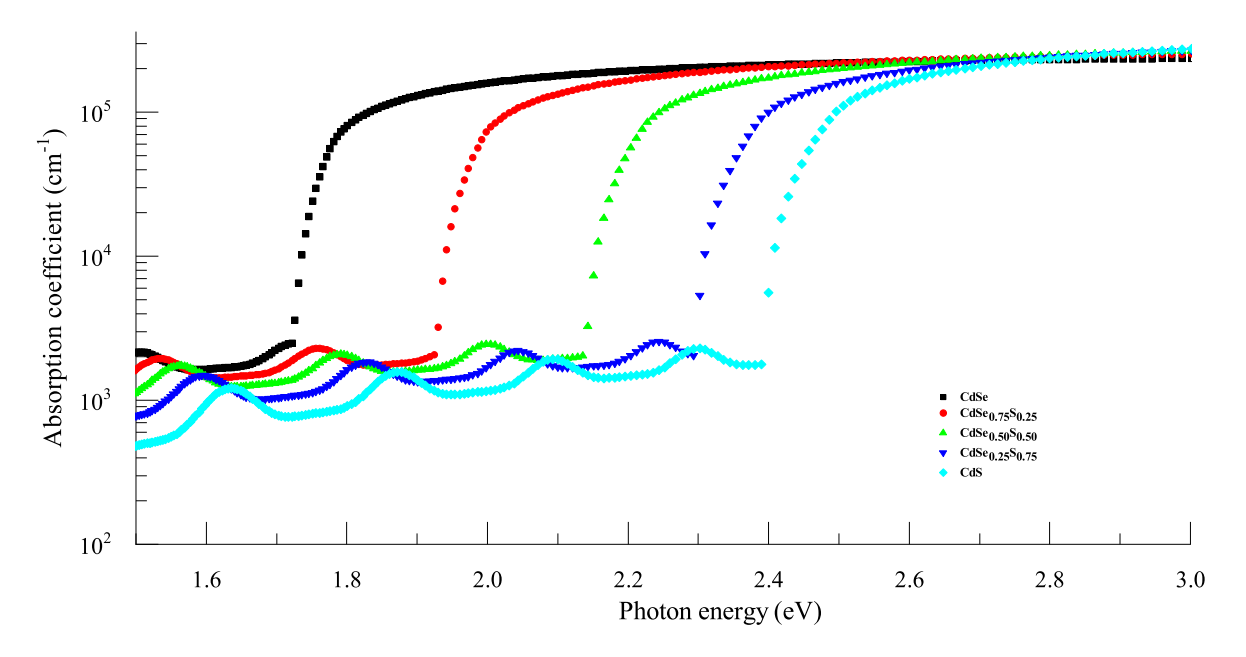


**Fig. 5:** The calculated absorption coefficient of  $CdSe_{1-x}S_x$  films/flexible substrates.

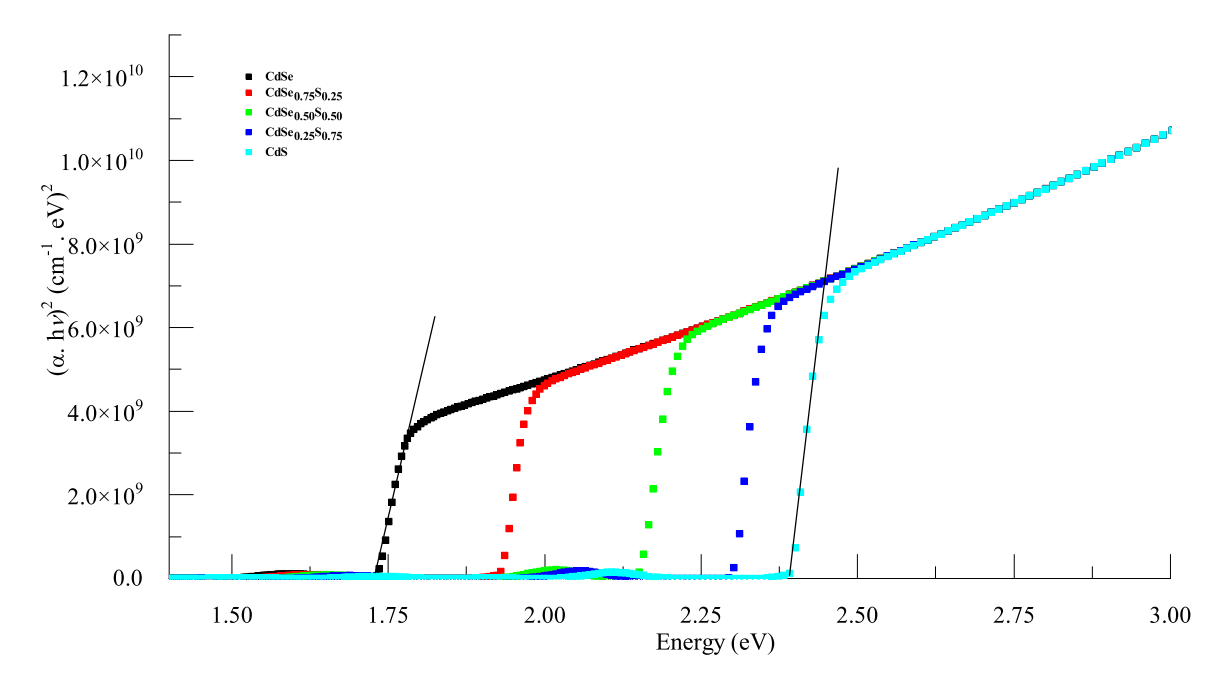


**Fig. 6:** The calculated energy gaps of  $CdSe_{1-x}S_x$  films/flexible substrates.

# 3.4 Extinction Coefficient Analysis of $CdSe_{1-x}S_x$ Thin Films

The extinction coefficient (k), which quantifies the attenuation of electromagnetic waves within a material due to absorption and scattering, was calculated from the absorption coefficient ( $\alpha$ ) and the wavelength ( $\lambda$ ) of the incident light using the following relation:

$$k = \left(\frac{\alpha \cdot \lambda}{4\pi}\right) \tag{9}$$

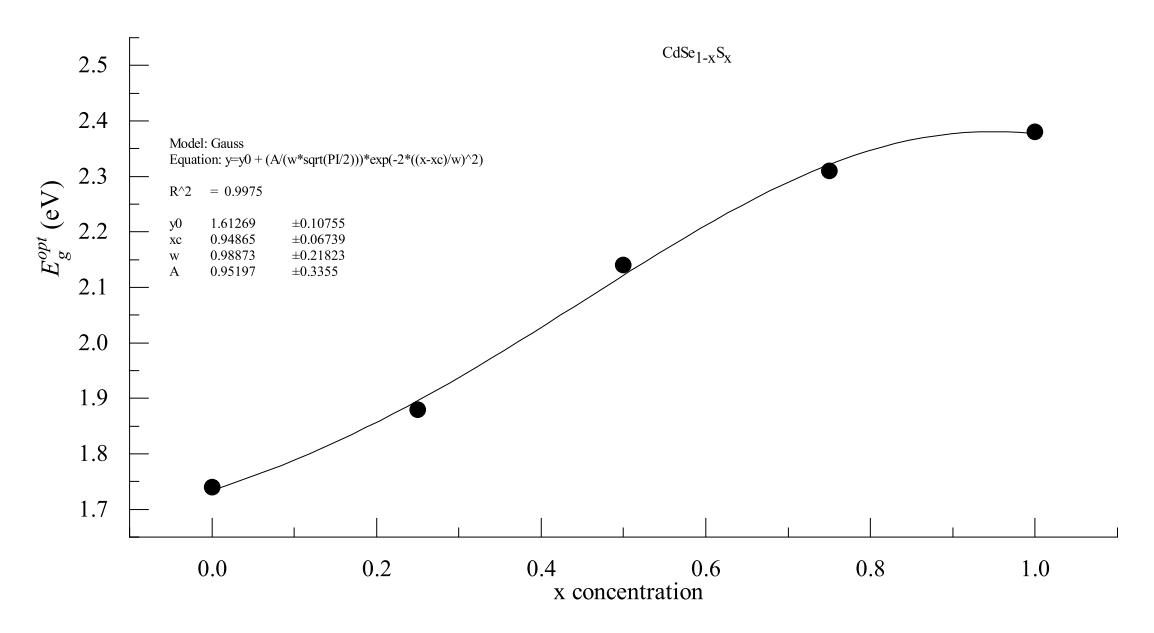


Fig. 7: Energy gap values as a function of x concentration of  $CdSe_{1-x}S_x$  films/flexible substrates.

Where:  $\alpha$  is the absorption coefficient (in cm<sup>-1</sup>),  $\lambda$  is the wavelength of the incident light (in cm) and  $\pi$  is the mathematical constant. Figure 8 illustrates the spectral dependence of the extinction coefficient for  $CdSe_{1-x}S_x$  thin films with varying sulfur content ( $0 \le x \le 10$ ). Each spectrum exhibits a prominent peak in the ultraviolet (UV) region, the position of which shifts systematically toward shorter wavelengths as the sulfur concentration increases. This blue shift in the peak position corresponds to a gradual increase in photon energy, from approximately 1.74eV (for pure CdSe) to 2.38eV (for pure CdS). The shift reflects the widening of the optical band gap as sulfur atoms progressively substitute selenium atoms in the alloy system.

The extinction coefficient is observed to be highest in the UV region, indicating strong optical absorption due to electronic transitions from the valence band to the conduction band. As the wavelength increases into the visible range, k decreases rapidly, suggesting reduced absorption and greater transparency. In the near-infrared (NIR) region, the extinction coefficient approaches zero, implying minimal photon absorption at longer wavelengths and highlighting the material's transparency in this spectral region. This spectral behavior of the extinction coefficient is closely related to the variation in the absorption coefficient and transmittance spectra of the films. In regions where the absorption coefficient is low, particularly in the visible and NIR zones, the transmittance is relatively high, resulting in a low extinction coefficient. Conversely, in the UV region where strong absorption dominates, the extinction coefficient reaches its maximum. This inverse relationship between transmittance and extinction coefficient underlines the consistency and accuracy of the optical measurements. Overall, the observed trends confirm the high optical quality of the  $CdSe_{1-x}S_x$  thin films and demonstrate how compositional tuning (i.e., adjusting sulfur content) can be used to engineer the optical attenuation properties of the material across different spectral regions.

# 3.5 Refractive Index Determination of $CdSe_{1-x}S_x$ /flexible substrate using classical method

The refractive index (n) is a fundamental optical property that significantly influences the performance of semiconductor materials in various photonic and optoelectronic applications, including light-emitting diodes (LEDs), photovoltaic devices, antireflective coatings, and display technologies. For this reason, accurate determination of nnn across the spectral range is essential for assessing the suitability of  $CdSe_{1-x}S_x$  thin films in such applications. The refractive index was calculated using the classical Fresnel equation, which relates the optical reflectance (R), refractive index (n), and extinction coefficient (k) through the following relation [31]:

$$R = \frac{(n-1)^2 + k^2}{(n+1)^2 + k^2} \tag{10}$$



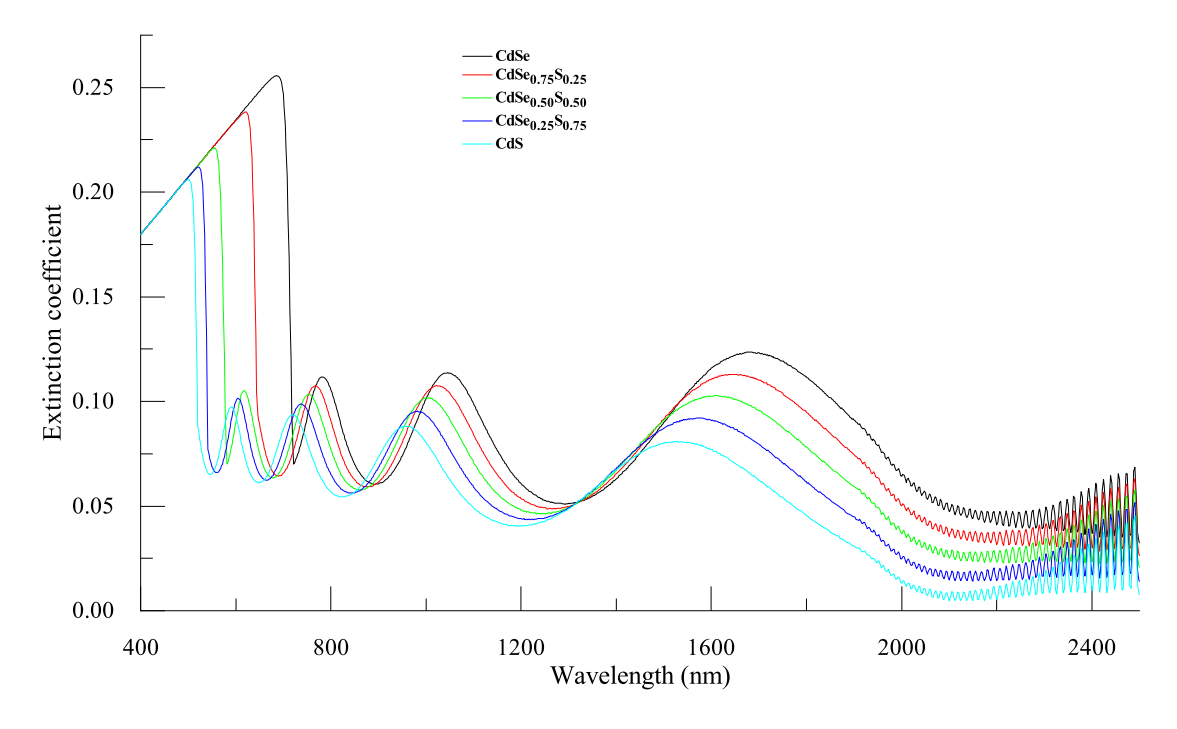


**Fig. 8:** Extinction coefficient of  $CdSe_{1-x}S_x$  films/flexible substrates.

By rearranging the Fresnel expression and applying standard algebraic transformations, the refractive index can be isolated and expressed as [29]:

$$n = \frac{(1+R)}{(1-R)} + \sqrt{\left(\frac{4R}{(1-R)^2} - k^2\right)}$$
 (11)

In this study, the values of n for the  $CdSe_{1-x}S_x$  thin films were computed using Eq. (11), based on experimentally obtained reflectance (R) and extinction coefficient (k) data. The variation of n with wavelength for different sulfur compositions ( $0 \le x \le 10$ ) is illustrated in Fig. 9. All compositions display an oscillatory behavior typical of interference effects in thin films.

A notable trend observed in all samples is that the refractive index decreases with increasing wavelength displays a behavior consistent with normal dispersion. This wavelength dependence can be described using the Cauchy dispersion relation, which is commonly applied to transparent materials in the visible and near-infrared spectral regions:

$$n(\lambda) = A + \frac{B}{\lambda^2} + \frac{C}{\lambda^4} \tag{12}$$

Where A, B, and C are material-specific Cauchy constants, and  $\lambda$  is the wavelength. However, to accurately extract the refractive index values in the medium and transparent regions of the spectrum, where the interference fringes are well-defined, the Swanepoel method was employed. This method is well-suited for thin-film systems and provides a more precise estimation of n by analyzing the envelope of the transmission spectrum. The Swanepoel approach is particularly effective when applied to interference fringes observed in the transparent and semi-transparent regions, where absorption is minimal. In conclusion, the refractive index of  $CdSe_{1-x}S_x$  thin films exhibits a composition and wavelength-dependent behavior, aligning well with theoretical models for thin-film optics. The combination of Fresnel's formulation and the Swanepoel method offers a comprehensive approach to characterize the optical constants of the material with high accuracy.

# 3.6 Determination of the Refractive Index of $CdSe_{1-x}S_x$ Thin Films on Flexible Substrates Using Swanepoel's Envelope Method

The refractive index (n) is a fundamental optical parameter that plays a critical role in determining the interaction of electromagnetic radiation with materials. It directly reflects the electronic polarizability of constituent ions and the



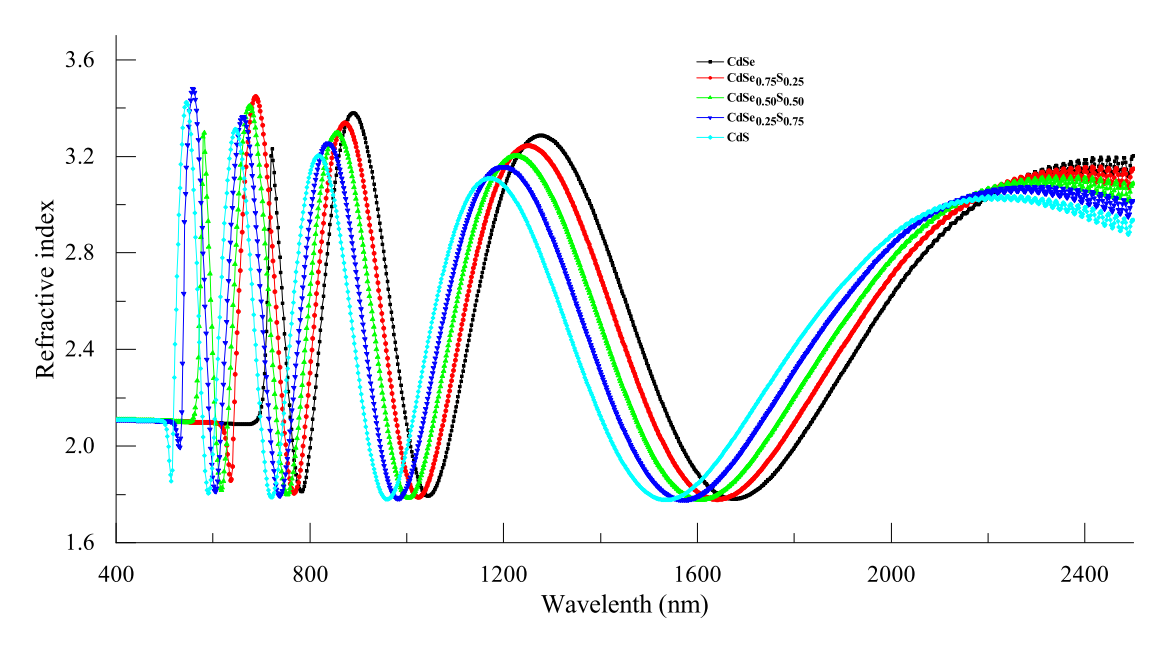


**Fig. 9:** The calculated refractive index of  $CdSe_{1-x}S_x$  films/flexible substrates.

internal electric field distribution within the material, thereby influencing its suitability for optoelectronic applications. In the present study, the refractive index of  $CdSe_{1-x}S_x$  thin films deposited on flexible substrates was determined through analysis of transmission spectra using Swanepoel's envelope method, a widely accepted technique for characterizing thin-film optical constants based on interference patterns in transmittance spectra. This method involves constructing envelopes around the interference maxima ( $T_{max}$ ) and minima ( $T_{min}$ ) observed in the measured transmission data. As an illustrative case, Fig. 10 presents the application of this method to the transmission spectrum of a  $CdSe_{1-x}S_x$  film. The same approach was systematically applied to samples of varying composition across the full compositional range ( $0 \le x \le 1$ ) of the  $CdSe_{1-x}S_x$  alloy system.

Using Swanepoel's formalism, the refractive index at any wavelength  $(\lambda)$  can be extracted using the following expression [29]:

$$n = \left[N + \left(N^2 - s^2\right)^{1/2}\right]^{1/2} \tag{13}$$

and

$$N = 2s \frac{T_{\text{Min}} - T_{\text{min}}}{T_{\text{Min}} T_{\text{min}}} + \frac{s^2 + 1}{2} \quad , \quad s = \frac{1}{T_s} + \left(\frac{1}{T_s^2}\right)^{1/2}$$

Where,  $T_{\text{max}}$  and  $T_{\text{min}}$  are the interference fringes maxima and minima, respectively; s is the refractive index of the substrate.

Additionally, the film thickness (d) was evaluated using the positions of adjacent interference extrema (either maxima or minima) in the spectrum, using the following relation:

$$d = \frac{\lambda_1 \lambda_2}{2(\lambda_2 n_1 - \lambda_1 n_2)} \tag{14}$$

Where  $n_2$  and  $n_1$  are the refractive indices at wavelengths  $\lambda_1$  and  $\lambda_2$ , respectively. The calculated film thicknesses for all compositions were found to be approximately 500 nm. In terms of the least squares fit of the two sets of values of n for the different composition of  $CdSe_{1-x}S_x$  (with  $0 \ge x \ge 1$ ) thin films, the fitted Cauchy parameters for the various compositions are as follows:

- -CdSe:  $n(\lambda) = 2.48 + (1.84 \times 10^5) / \lambda^2$
- -CdSe <sub>0.25</sub> S<sub>0.75</sub>:  $n(\lambda) = 2.43 + (1.85 \times 10^5) / \lambda^2$
- -CdSe<sub>0.50</sub>S<sub>0.50</sub>:  $n(\lambda) = 2.36 + (1.87 \times 10^5)/\lambda^2$
- -CdSe0.75S0.25:  $n(\lambda) = 2.32 + (1.88 \times 10^5) / \lambda^2$

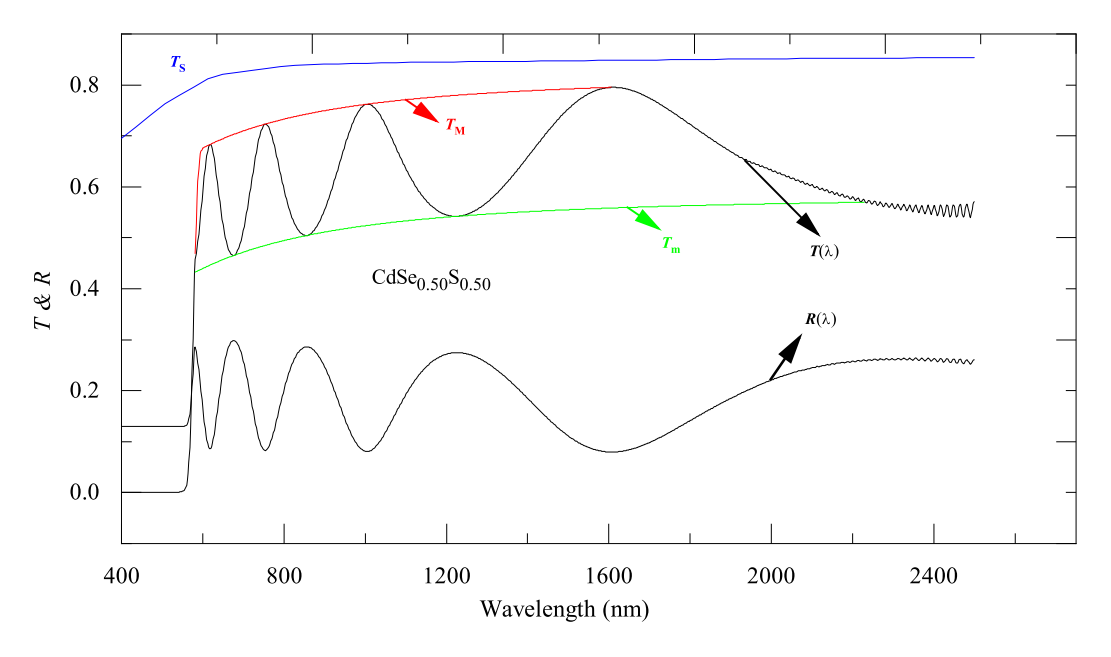


**Fig. 10:** Both T and R spectra for CdSe<sub>0.5</sub>S<sub>0.5</sub>,  $T_M$ ,  $T_m$  and  $T_s$  according to the text.

-CdS: 
$$n(\lambda) = 2.27 + (1.85 \times 10^5) / \lambda^2$$

As evident from the Cauchy parameters [32, 33], there is a systematic decrease in the refractive index as the sulfur concentration increases (see Fig. 11). This behavior is consistent across the entire spectral range studied and can be attributed primarily to the intrinsic differences in the atomic polarizability and ionic radius of selenium and sulfur atoms.

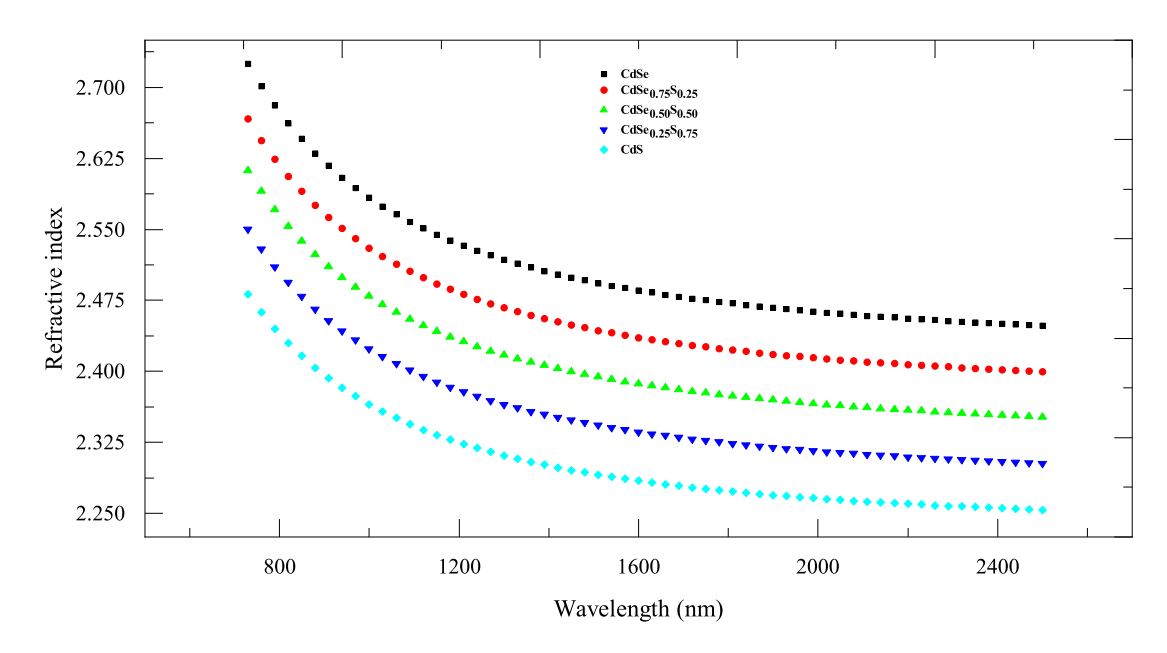


Fig. 11: The refractive index as a function of wavelengths of  $CdSe_{1-x}S_x$  films/flexible substrates.

Selenium (Se), which has a larger ionic radius ( $\sim$  198 pm) and higher electronic polarizability compared to sulfur (S) ( $\sim$  184 pm), contributes more significantly to the overall dielectric response of the material. The greater polarizability of



Se allows its electron cloud to distort more easily under the influence of an external electric field, thereby increasing the material's refractive index. Conversely, substituting Se with the smaller and less polarizable S atoms reduces the material's ability to respond to optical fields, resulting in a lower refractive index. Additionally, the substitution of Se with S leads to a modification of the local electronic structure, including changes in bond lengths and lattice distortion, which further affects the dielectric properties. The smaller atomic size of S leads to a more tightly bound electron cloud, reducing the contribution of electronic polarization to the material's optical constants. This effect becomes more pronounced with increasing sulfur content, as reflected in the gradual decrease of the fitted Cauchy coefficient a. Therefore, the observed trend in the refractive index with varying composition is a direct consequence of the interplay between atomic size and polarizability of the anions in the  $CdSe_{1-x}S_x$  alloy system. These findings highlight the ability to fine-tune the optical properties of II–VI semiconductor thin films through targeted compositional engineering, offering potential for optimized performance in photonic and optoelectronic devices.

#### 4 Conclusions

The fabrication and in-depth characterization of  $CdSe_{1-x}S_x$  thin films on polymer substrates revealed notable effects of sulfur incorporation on the material's microstructure and optical performance. Structural analysis showed that sulfur substitution leads to lattice compression, evident from the systematic reduction in crystallite size and lattice constants, alongside an increase in internal strain. These modifications stem from the smaller ionic radius and higher electronegativity of sulfur relative to selenium. Optical studies demonstrated a consistent increase in band gap energy with higher sulfur content, resulting from both nanoscale quantum confinement and changes in the material's electronic configuration. Additionally, optical constants such as the extinction coefficient and refractive index followed expected dispersion trends and were reliably quantified using established optical models. Overall, the results confirm that the  $CdSe_{1-x}S_x$  system can be compositionally tailored to achieve desired structural and optical properties, offering considerable promise for use in next-generation, flexible optoelectronic applications.

#### **Conflict of Interest**

The authors declare that there is no conflict of interest regarding the publication of this paper.

#### References

- [1] M. A. Abbas and R. Mohamed, Thermal evaporated cdse thin films: Optical absorption and photoresponse characteristics, *Journal of Alloys and Compounds* **921** (2023) p. 167107.
- [2] J. M. Al-Abbasa, H. M. Badran and D. J. Smith, Phase composition and band gap tuning in spray pyrolyzed cdse thin films, *Chalcogenide Letters* **20**(5) (2023) 209–217.
- [3] M. M. Rahman and S.-H. Lee, Low-temperature synthesis (†100 °c) of nanostructured cdse films for solar applications, *Frontiers in Chemistry* **9** (2021) p. 661723.
- [4] O. Karkulovska, E. Ivanova and O. Petrenko, Composition-controlled growth of magnetron-sputtered  $cdse_{1-x}s_x$  films for optoelectronic applications, *Ukrainian Journal of Physics* **68**(10) (2023) 905–912.
- [5] F. Fan, Y. Ren, Y. Dang and Y. Liu, Colloidal  $cdse_{1-x}s_x$  nanoplatelets: Tunable electroluminescence across visible wavelengths, *Nano Letters* **15**(12) (2015) 8039–8045.
- [6] F. Banyai and V. Rusu, Structural and optical properties of thermally evaporated cdse thin films, *Thin Solid Films* **441**(1–2) (2003) 123–127.
- [7] J. H. Lee, S. Park and K. Kim, Refractive index and extinction coefficient of pld-grown cdse on ito, *Materials* **14**(12) (2021) p.
- [8] Y. Chen and X. Sun, Advances in vacuum and chemical vapor deposition of semiconductor thin films, *Processes* **13**(2) (2023) p. 587
- [9] J. M. Al-Abbasa, S. El Sawy and H. M. Badran, Structural phase evolution and optical gaps in cdse by spray pyrolysis, *Chalcogenide Letters* **20**(7) (2023) 301–310.
- [10] L. Zhang and P. Wu, Application of swanepoel's envelope method in ii vi thin-film optical study, *Optical Materials* **124** (2022) p. 112065.
- [11] M. M. Rahman and S.-H. Lee, Low temperature deposition techniques for flexible optoelectronic systems, *Frontiers in Chemistry* **9** (2021) p. 661723.
- [12] Q. He and R. Süsstrunk, Zinc oxide based flexible electronics: A review, *Materials Science in Semiconductor Processing* **70** (2017) 178–189.



- [13] J. M. Al Abbasa, H. M. Badran and A. M. Farag, Microstructural effects of process temperature in cdse thin films, *Journal of Electronic Materials* **52**(4) (2023) 2456–2465.
- [14] Y. Chen and X. Sun, Effects of deposition parameters on interface microstructure in ii–vi thin films, *Processes* 13(2) (2023) p. 587.
- [15] M. M. Rahman and S.-H. Lee, Bandgap tuning in cdse thin-film solar harvester, Frontiers in Chemistry 9 (2021) p. 661723.
- [16] A. S. Patel and N. Joshi, Spectroscopic and refractive index dispersion analyses of cdse thin films, *Journal of Optoelectronics and Advanced Materials* **23**(9–10) (2021) 512–520.
- [17] F. Fan, Y. Ren, Y. Dang and Y. Liu, Visible-light-emitting cdse<sub>1-x</sub>s<sub>x</sub> nanoplatelets, *Nano Letters* **15**(12) (2015) 8039–8045.
- [18] J. M. Al Abbasa and H. M. Badran, Spray pyrolyzed cdse for solar relevant absorption and stability, *Chalcogenide Letters* **20**(8) (2023) 345–353.
- [19] Y. Chen and X. Sun, Engineering optical constants of ii–vi thin films for photovoltaic applications, *Processes* 13(2) (2023) p. 587.
- [20] B. D. Cullity, Elements of X-ray Diffraction, 2nd edn. (Addison-Wesley, 1978). No DOI.
- [21] G. K. Williamson and W. H. Hall, X-ray line broadening from filed aluminium and wolfram, Acta Metallurgica 1 (1953) 22–31.
- [22] H. Bragg and W. L. Bragg, The reflection of x-rays by crystals, Proceedings of the Royal Society of London A 88 (1913) 428–438.
- [23] M. Mahdi *et al.*, Structural and optical properties of  $cdse_{1-x}s_x$  thin films, *Journal of Materials Science: Materials in Electronics* **25** (2014) 1908–1915.
- [24] S. Rajendran et al., Influence of s incorporation on cdse thin films, Materials Chemistry and Physics 120(1) (2010) 335-341.
- [25] Y. Wang et al., Effect of strain on grain growth in nanostructured films, Thin Solid Films 520(6) (2012) 1913–1918.
- [26] L. Vegard, Die konstitution der mischkristalle und die raumfüllung der atome, Zeitschrift für Physik 5 (1921) 17–26.
- [27] C. Wolden et al., Chemical bonding and structural evolution in cdse and cds systems, Journal of Applied Physics 105 (2009) p. 083543.
- [28] M. S. Islam *et al.*, Optical and structural characterization of  $cdse_{1-x}s_x$  nanostructures, *Semiconductor Science and Technology* **30**(3) (2015) p. 035015.
- [29] M. El-Hagary, M. Emam-Ismail, E. R. Shaaban and A. El-Taher, Effect of  $\gamma$ -irradiation exposure on optical properties of chalcogenide glasses  $se_{70}s_{30-x}sb_x$  thin films, *Radiation Physics and Chemistry* **81**(10) (2012) 1572–1577.
- [30] J. I. Pankove, Optical Processes in Semiconductors (Courier Corporation, 1975).
- [31] G. García and J. J. Sánchez-Mondragón, Fresnel equations and the refractive index of active media, *Physical Review E* **73**(2) (2006) p. 026605.
- [32] E. R. Shaaban, M. N. Abd-el Salam, M. Mohamed, M. A. Abdel-Rahim and A. Y. Abdel-Latief, Optical characteristics of some chalcogenide glasses, *Journal of Materials Science: Materials in Electronics* 28(19) (2017) 13379–13388.
- [33] E. R. Shaaban, M. M. Mahasen, M. M. Soraya, E. S. Yousef, S. A. Mahmoud, G. A. Ali and H. A. Elshaikh, Optical analysis of se-te-sn thin films, *Journal of the American Ceramic Society* **102**(7) (2019) 4067–4078.